A Novel Enhanced-Performance Flexible RFID-Enabled Embroidered Wireless Integrated Module for Sensing Applications

Masoumeh Hasani, *Student Member, IEEE*, Arnaud Vena, *Member, IEEE*, Lauri Sydänheimo, *Member, IEEE*, Manos M. Tentzeris, *Fellow, IEEE*, and Leena Ukkonen, *Member, IEEE*

***Abstract*— A novel wireless embroidered integrated platform for radio frequency identification (RFID)-enabled strain sensing that takes advantage of the nonlinear behavior of the RFID chip impedance as a function of the incident power is introduced. Due to the nonlinearity of the chip impedance as a function of the power, a large variation of chip impedance value and thus a large difference of radar cross section values for appropriately chosen power levels are achieved. Taking advantage of this idea, the sensing parameter is detected by interrogation of the sensor tag using two distinct transmitting power levels and calculating the difference of backscattered response. As a proof of concept, we applied the proposed method for the detection of an embroidered RFID-enabled strain sensor that is fabricated using electrotextiles in order to observe the variations of the magnitude and the corresponding strain levels. The proposed model for the chip impedance helps in predicting the RFID chip impedance variation for different strain conditions, an extremely important issue for RF/RFID modules and packages operating over a wide power dynamic range as well as enabling the accurate estimation of the maximum range of the RFID-enabled sensing modules for the maximum allowable power levels.**

***Index Terms*— Chip impedance, double power, embroidered sensors, nonlinearity, radar cross section (RCS), radar techniques, radio frequency identification (RFID), strain sensors, Tagformance, wireless.**

I. Introduction

RADIO frequency identification (RFID)-enabled sensors have become increasingly attractive over the recent years [1]–[3], especially motivated by the principles of the Internet of Things and of Smart Skins being sought after by numerous companies. This concept relies upon the deployment of tens of billions of interconnected sensors for environment, comfort, and safety purposes.

Manuscript received January 2, 2015; revised May 9, 2015 and July 11, 2015; accepted July 12, 2015. Date of publication August 19, 2015; date of current version September 18, 2015. This work was supported in part by the U.S. National Science Foundation, in part by the Finnish Funding Agency for Technology and Innovation, and in part by the Academy of Finland. Recommended for publication by Associate Editor P. Franzon upon evaluation of reviewers' comments.

M. Hasani, L. Sydänheimo, and L. Ukkonen are with the Tampere University of Technology, Tampere 33720, Finland (e-mail: masoumeh.hasani@tut.fi; lauri.sydanheimo@tut.fi; leena.ukkonen@tut.fi).

A. Vena is with the Université Montpellier 2, Montpellier 34000, France (e-mail: arnaud.vena@univ-montp2.fr).

M. M. Tentzeris is with the Georgia Institute of Technology, Atlanta, GA 30332-250 USA (e-mail: etentze@ece.gatech.edu).

Color versions of one or more of the figures in this paper are available online at http://ieeexplore.ieee.org.

Digital Object Identifier 10.1109/TCPMT.2015.2461661

RFID technology provides some good arguments to compare with other wireless technologies. Mainly, the fact that a passive tag does not require any battery to operate is a feature of significant importance to deploy large-scale networks of RFID sensors [4], [5]. This dramatically decreases the maintenance cost that is usually due to the replacement of battery cells in transponders.

A typical passive RFID tag is composed of a chip connected to an antenna with a matching circuit. An RFID sensor tag can be fabricated in a way that either the antenna or the matching circuit's electrical/electromagnetic (EM) performance be sensitive to changes of the sensed parameter. As it is reported in [6], for gas or humidity sensors, the sensing technique consists of the deposition of a film of a sensitive material with a complex permittivity value varying as a function of the concentration of the physical parameter to detect. For numerous antenna-based strain sensors, the electrical length and width of the antenna are correlated with the strain value [7], [15].

The commonly used techniques for passive RFID sensors have been introduced in [8]–[10]. An analog approach [8], [9] relies upon the monitoring of values of transmitted power to activate the tag or the backscattered power from the tag to track the evolution of a physical parameter. In the case when only two states have to be distinguished, such as detecting if a liquid container is filled or not, a simpler technique can be used as in [10].

One of the main challenges of using such a sensor platform in rugged environment in the presence of ambient scatterers is the high-accuracy detection of the sensed parameters. In addition, for numerous end-user applications, such as wireless sensor networks, the maximum detection range of the sensor is significant as well. Here, we propose an integrated approach to identify the nonlinear variation of the IC chip impedance for different transmitted power levels—a critical issue in most RFID and RF modules and packages operating at various power levels—as well as an integrated wireless platform that could exploit this nonlinearity for the detection of the RFID-enabled sensor tags.

As it has been reported in [11], one of the techniques to detect these types of sensors is based on the measurement of the tag's radar cross section (RCS) that is mostly used in the identification of chipless tags [14], [17]. Based on the

results presented in [11], the advantages of utilizing an RCS-based technique are the simplicity and the lack of the need for specific protocols for the detection of the sensed parameters. However, the detection of the sensor in highly cluttered indoor environments requires an accurate calibration process to remove all static reflections from the ambient scatterers [12]. This makes the detection process quite time consuming and complex, as it is already discussed in [18].

This paper addresses this problem taking benefit of the nonlinearity of the RFID chip by introducing an estimated model of chip impedance as a function of the transmitted power, which also allows predicting the maximum read range of the detection method. The nonlinear behavior of chip causes a large variation of its impedance value as a function of the received power. The RFID tag presents a certain RCS value due to the impedance variation, and the difference provided between the high and low impedance backscattered signal is noted ΔRCS ($|\sigma_{\max} - \sigma_{\min}|$). The RFID-enabled sensor is detected by transmitting two distinct powers that can guarantee a large variation of chip impedances consequently the RCS. The novel detection method introduced in this paper allows cancelation of the background response, taking benefit from this chip nonlinearity.

In Section II, we present the extraction of the chip impedance as a function of the transmitted power based on the RCS measurements and simulations. Then, in Section III, the estimated impedance model is expanded for other measurement ranges and power levels. A discussion about how this model can be utilized for the estimation of the maximum read range of the double-power detection method is covered in Section IV. The validity of the proposed model using the Tagformance measurement setup is presented in Section V, before closing with the conclusions in Section VI.

II. Extraction of the Chip Impedance as a Function of the Transmitted Power

The double-power measurement technique as a novel measurement method for the detection of the sensor tags was already introduced in [18]. Since the idea behind the method comes from the nonlinear behavior of the impedance of the RFID chip as a function of the transmitted power, here, more detail of this issue is discussed.

Basically, in this section, we will describe how the impedance of the RFID chip varies as a function of the transmitted power and causes different RCSs of the tag and makes the different responses of the tag happen. The accurate prediction and estimation of this nonlinearity could find numerous applications, such as the design of integrated time-reconfigurable matching circuits for different power levels as well as the RF module performance optimization over large power dynamic ranges.

To demonstrate the proof of concept, we first measured the chip impedance of a simple dipole tag [Fig. 1(a)] using a monostatic radar measurement setup [Fig. 1(b)]. Utilizing the measurement results and correlation with the simulation, an estimated model for the chip impedance as a function of the transmitted power has been achieved. This model also provides us the changes of the RCS of the tag as a function of the chip impedance for a fixed distance. Then, to generalize this impedance model for the other distances, the chip impedance has also been measured utilizing the vector network analyzer (VNA).

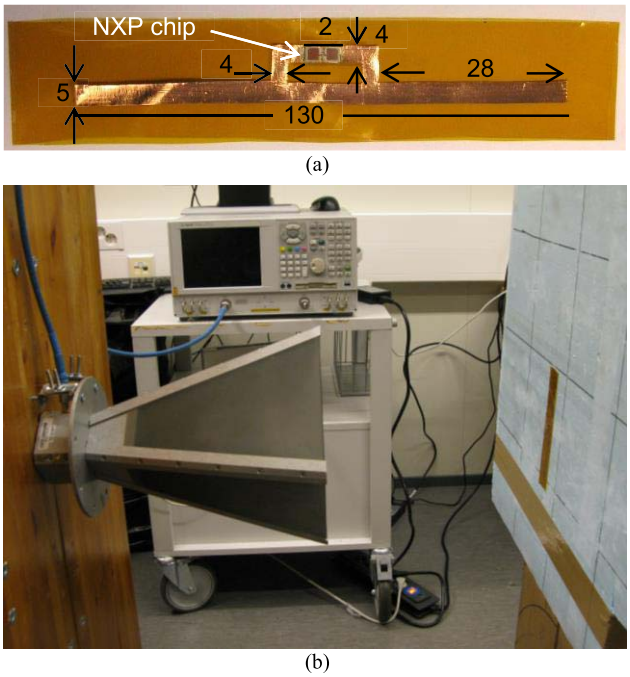

Fig. 1. (a) Copper-based RFID tag. (b) Monostatic RCS measurement setup.

Based on the achieved models for the RCS (as a function of the chip impedance) and the chip impedance (as a function of the transmitted power), the maximum read range of the proposed technique has been estimated. The estimation is experimentally verified by the detection of a strain sensor tag in different distances.

To study the behavior of the chip impedance as a function of transmitted power, an impedance measurement method has been introduced in this section. For this paper, we used the chip NXP UCODE G2iL SL3S1203AC0 having a sensitivity of -18 dBm. The chip is attached to a dipole antenna using the conductive epoxy. The dipole is a pure copper conductor tape that is applied on the top of a polyimide-based thin substrate. The prototype sample is shown in Fig. 1(a). The procedure for measuring the impedance is described in the following.

A. RCS Measurement of the Tag

In the first step of the impedance measurement, the RCS of the tag has been measured using a frequency-domain measurement setup. As it is shown in Fig. 1(b), the tag is placed on Styrofoam stand at a distance of 20 cm from the horn antenna. This measurement distance, as an initial range, has been optimized based on the power levels and to speed up the measurement. This issue will be discussed in more detail in the following sections. The dual-polarization wideband horn antenna ETS Lindgren 3164-04 is connected to a two-port VNA Agilent PNA E8358A. To cover the whole UHF-RFID band, the frequency is adjusted from 800 to 980 MHz. The power delivered by the VNA varies

from −14 to +14 dBm with 2-dBm steps. Due to the limitation of the available VNA, the maximum power level cannot exceed +14 dBm. Thus, the minimum power level and the power steps have been adjusted to have a reasonable power resolution for the measurements.

Since the tag is placed vertically in front of the reader antenna and it is matched with the vertical polarization of horn antenna, only port 1 of VNA is connected to the vertical polarization input of the antenna. Thus, the measured scattering parameter S_{11} contains the EM response of the tag in vertical polarization.

To remove the effect of unknown objects around the measurement setup, and keep only the tag response, a calibration process is applied. Thus, in addition to the tag measurement for the whole frequency band in a specific transmitted power, a no-tag measurement has been performed to remove all static reflections from the environment. Moreover, a measurement with a reference scatterer (a metallic rectangular plate) is performed to compensate the filtering effect from the antenna, the cables, and the free-space channel. Finally, the no-tag measurement is subtracted from the tag measurement and divided by the reference sample measurement. This technique allows extracting the tag response clearly even outside the anechoic chamber [12]. Since the RCS value of the metallic reference sample σ_{ref} is known according to the analytical equations, it is possible to calculate the value of the RCS for the tag for every transmitted power level as follows [12]:

$$\sigma_{\text{tag}} = \left[\frac{S_{11_{\text{tag}}} - S_{11_{\text{no-tag}}}}{S_{11_{\text{ref}}} - S_{11_{\text{no-tag}}}}\right]^2 \cdot \sigma_{\text{ref}}. \tag{1}$$

Based on (1), the RCS values of the tag for all transmitted power and frequency values have been plotted in Fig. 2(a). The curves show the change of RCS values corresponding to different transmitted power levels in a measured frequency band. To have the best interpretation of the results, the RCS values for the peak-RCS frequency point (915 MHz) is considered here. The absolute value of the measured RCS at 915 MHz as a function of the transmitted power has been plotted in Fig. 2(c).

B. RCS Simulation of the Tag

To extract a model of the chip impedance as a function of the power, we used a retrosimulation technique in order to find the parameters that allow getting the results very close to the measured ones. The RCS value of the same tag [Fig. 1(a)] has been simulated using CST Microwave studio. To model the chip in simulation, a parallel lumped element circuit has been connected to the output port of the antenna. As it is shown in Fig. 3(a), the chip connected to the tag antenna is modeled as a resistance R_{chip} in parallel with a capacitor C_{chip}. The total impedance of the equivalent circuit model is defined as

$$Z_{\text{chip}} = \frac{R_{\text{chip}} \cdot X_{\text{chip}}}{R_{\text{chip}} + X_{\text{chip}}} \tag{2}$$

where $X_{\text{chip}} = 1/(j \cdot \omega \cdot C_{\text{chip}})$.

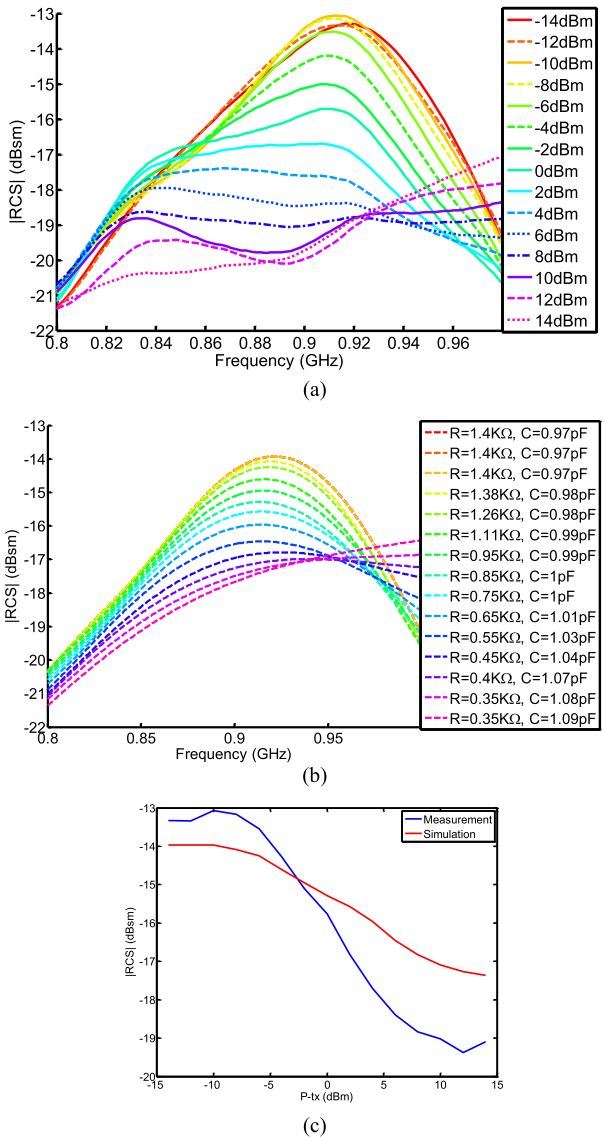

Fig. 2. (a) RCS measurement results as a function of transmitted power P_{tx} and frequency. (b) Most similar simulated RCS to the measurement results. (c) RCS versus the P_{tx} at 915 MHz.

The simulated RCS curves of the tag corresponding to a normally incident plane wave, which relies upon a monostatic radar technique, is achieved by changing the values of R_{chip} and C_{chip}. To get a good agreement between the simulated and measured RCS, the R_{chip} varies from 300 to 2800 Ω with a step of 50 Ω. Simultaneously, C_{chip} evolves from 0.9 to 1 pF with a step of 0.01 pF. Thus, finally, 1600 different RCS curves are obtained using the simulation.

C. Comparison of the Simulation and Measurement Results

The final step of impedance extraction of the chip is comparing the results of the simulation with those of the measurement. Using MATLAB for post-processing calculation, a least-square method allows finding the parameters that minimize the error between a given measurement result, and its closest simulation result amid 1600 curves, for the whole power and frequency range. Fig. 2(b) shows a subset of the simulated RCS curves that are the most similar to the measurement results shown in Fig. 2(a).

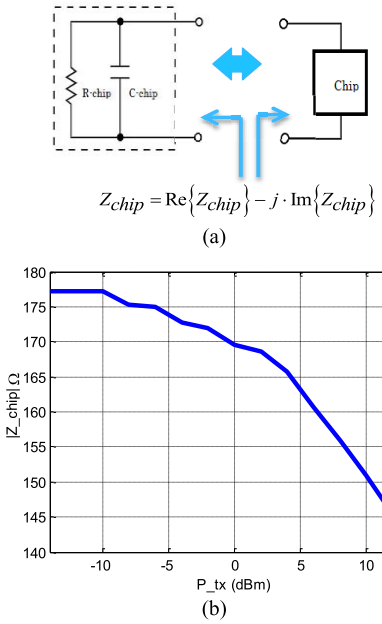

Fig. 3. (a) Equivalent circuit model of the chip used for simulation. (b) Impedance of the chip as a function of transmitted power P_{tx}, which is extracted with the help of measurement and simulation.

As it is shown in Fig. 2(b), each RCS curve is associated with a specific R, C values that minimize the error with a measured RCS curve recorded for a specific transmitted power. Correlation between the simulation and measurement curves gives the equivalent transmitted power for each R_{chip} and C_{chip} (in other words, Z_{chip}).

Utilizing this method, we were able to derive a relationship between the transmitted power levels toward the tag (P_{tx}) and the value of its chip impedance (Z_{chip}). This relationship has been plotted in Fig. 3(b), and it is dependent from the measurement distance and the minimum and maximum levels of transmitted power. As one can see, when the transmitted power is too low (less than -10 dBm), with respect to the measurement distance (20 cm) and sensitivity of the chip (-18 dBm), the chip is not activated, and the absolute value of the chip impedance is constant (about 178 Ω). By increasing the transmitted power, we activate the chip, and the absolute value of its impedance reduces to around 140 Ω.

The VNA that has been used for this measurement can transmit a stable (high amplitude stability) power until 15 dBm. This gives the upper limit to the power that we can transmit for the chip model extraction. Consequently, it was not possible to plot the behavior of the impedance for higher power values, but extrapolation should be considered according to the curve shape for the power levels below -10–15 dBm.

As the behavior of the chip impedance shows, there are minimum and maximum impedance states corresponding to the lower and the upper limits of the transmitted power. For each impedance state, the RFID tag presents a certain RCS value that is described as follows [13]:

$$\sigma = \frac{\lambda^2 \cdot G_{\text{tag}}^2 \cdot R_a^2}{\pi \cdot |Z_a + Z_{\text{chip}}|^2} \tag{3}$$

TABLE I
SYSTEM PARAMETERS

Parameter	Description	Value at 915 MHz
G_{horn}	Gain of horn antenna (datasheet)	5.5 dBi
G_{tag}	Gain of tag antenna (simulated)	4.3 dBi
L_{cable}	Loss of cable connected between VNA and horn (measured)	0.5 dB
λ	Wavelength	0.327 m
r	Read distance	20 cm
P_{tx}	Transmitted power by VNA	-14 to +14 dBm

where $Z_a = R_a + j \cdot X_a$ is the impedance of the antenna of the tag, G_{tag} is the simulated gain of the tag, and λ is the wavelength. The values for the system parameters are available in Table I. The difference between the RCS at high- and low-impedance state is noted ΔRCS, which is somehow a similar concept to that of the backscattered signals in the protocol-based measurement method, except that the RCS state is not dynamically modified by the electronics of the chip.

The curves plotted in Fig. 2(c) show the RCS value from the measurement and simulation. The reason for small disagreement (about 1.5 dB) is due to the accuracy of measurement and also least-square method for finding the similar curves. The ΔRCS value of about 5.5 dB (from the measurement results) has been calculated between the minimum and maximum impedance states that are fitted properly with the equation described in (3).

III. STUDY OF THE IMPEDANCE MODEL FOR THE DIFFERENT MEASUREMENT DISTANCES

The estimated model of the chip impedance in Fig. 3(b) depends on the transmitted power levels and also the measurement distance, since the measurement is done wirelessly. To be able to generalize the impedance model for other power levels and the distances, the impedance of the chip has also been measured using a VNA as it is described in this section.

A. Chip Impedance Measurement Using VNA

The Agilent VNA E5071c is utilized for the impedance measurement of the chip. Before the actual measurement, ports 1 and 2 of the VNA are calibrated (to the end of blue cables) using the Agilent electronic calibration module N4431. In addition, the effect of the handmade SMA-fixture is taken into account using the port-extension option of the VNA. As it is shown in Fig. 4(a), left side, the chip mounted on the strap, is soldered to the SMA fixture and then connected to ports 1 and 2 of the VNA. The S-parameters of the chip for power varying from -20 to 4 dBm at a single frequency (915 MHz) is measured. The frequency of 915 MHz is considered as it is already explained in the previous section, to keep the results comparable. The impedance of the chip can be calculated using the measured S-parameters as follows:

$$Z_{11} = \frac{((1 + S_{11})(1 - S_{22}) + S_{12}S_{21})}{(1 - S_{11})(1 - S_{22}) - S_{12}S_{21}} Z_0 \tag{4}$$

where Z_0 is 50 Ω.

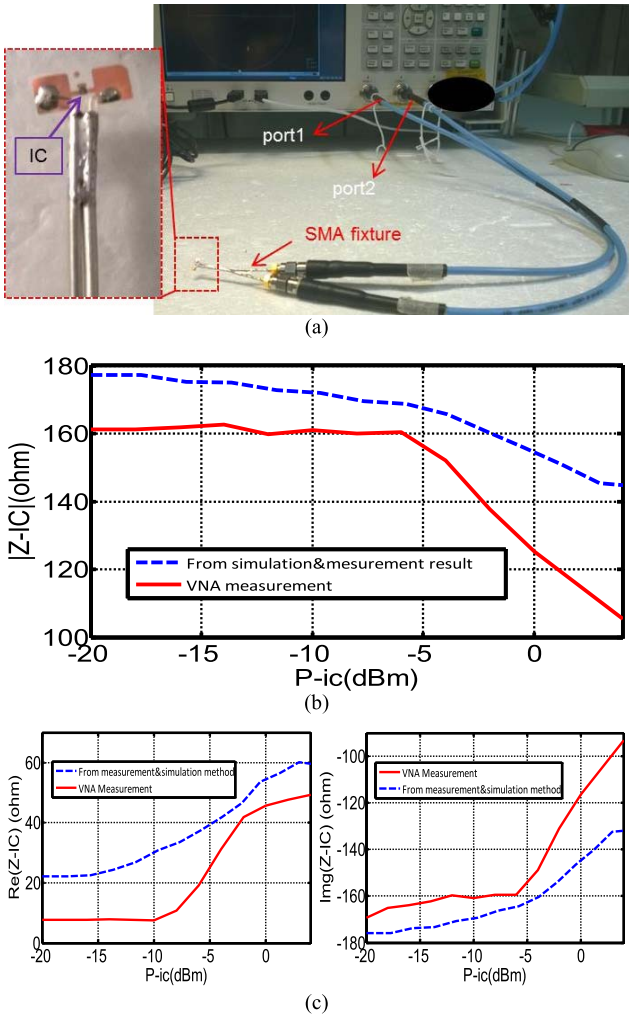

Fig. 4. (a) Setup for the measurement of the chip impedance. The comparison of the chip impedance result using VNA (solid lines) and measurement–simulation results (dashed lines), (b) absolute values, and (c) real and imaginary values. P-ic is equal with P_{chip} as mentioned in the text.

The solid lines in Fig. 4(b) and (c) show the absolute, real, and imaginary parts of the chip impedance, respectively, which is measured using the VNA. The dashed lines in Fig. 4(b) and (c) indicate the impedance parts achieved by a method in the previous section. Comparing the results in Fig. 4(b), there is a maximum 40-Ω offset between the curves. The disagreement can be explained by many reasons. First of all, in case of wireless measurement, the isolation obtained with the monostatic radar bench test is not ideal and this will slightly affect the S-parameter values. In addition, the chip connection to the antenna utilizing the conductive epoxy also adds parasitic components to the circuit model. The R, C model is a simplified equivalent compare to the actual chip model. Finally, the measurement misalignments and matching condition are other reasons that cause the disagreement. Despite this difference, both results prove the nonlinear behavior of the chip impedance as a function of the power, which is the significant conclusion of the measurements.

B. Estimated Model for Different Measurement Distances

The impedance model presented in Fig. 4(a) (solid lines) is only a function of the transmitted power and it is independent from the measurement distance. By utilizing this model and also the link budget calculations, we can extract the chip impedance behavior when both factors of distance and transmit power vary. Later, this model will be used to estimate the required power levels in higher read range for the detection of the sensor tag.

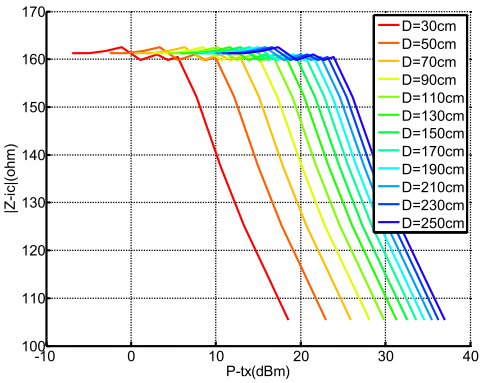

Fig. 5. Estimation of the chip impedance behavior for different transmitted power levels and different distances between tag and reader.

When the tag, shown in Fig. 1(a), is placed at a distance of 20 cm away from the reader antenna, for transmitted power levels P_{tx} between −14 and +14 dBm, the power absorbed by the tag is calculated using the Friis equation as follows:

$$P_{\text{tag}} = \frac{G_{\text{horn}} \cdot G_{\text{tag}}}{L_{\text{cable}}} \cdot \left(\frac{\lambda}{4\pi r}\right)^2 \cdot P_{tx} \tag{5}$$

where the parameters in (5) are defined in Table I. The gain of the tag has been calculated by the simulation. Not all the power absorbed by the tag will be transferred to the chip because of impedances' mismatch. The ratio of the absorbed power by the tag (P_{tag}) to the delivered power to the chip (P_{chip} or P-ic) is defined as follows:

$$\tau = \frac{P_{\text{chip}}}{P_{\text{tag}}} = \frac{4R_a R_{\text{chip}}}{|Z_a + Z_{\text{chip}}|^2} \tag{6}$$

where $Z_a = R_a + jX_a = 27 + j170$ is the tag antenna impedance at 915 MHz achieved from the simulation, and the chip impedance $Z_{\text{chip}} = R_{\text{chip}} + jX_{\text{chip}}$, that varies as a function of P_{tx}, is known from Fig. 4(b) (solid lines). After calculating P_{tag} using (5) and substituting Z_{chip}, Z_a, and P_{tag} in (6), the P_{chip} is calculated. By varying the transmitted power between −14 and +14 dBm, the P_{chip} changes from −21 to 5 dBm. Same power range has also been used for the measurement of the chip impedance by VNA [Fig. 4(b)].

Since we already know the nonlinear behavior of the impedance as a function of the P_{chip}, and assuming that the P_{chip} varies in the same range (−21–5 dBm), the transmitted power can be easily calculated using (6) and (5) when the read range (r) in (5) changes.

Fig. 5 shows the estimated impedance behavior of the chip as a function of the P_{tx} in different distances. As one can see, the transmitted power range should increase for larger distances to keep the impedance variation of the chip in the region that can guarantee the RCS variation, as it is plotted in Fig. 2(c).

In the following section, when the double-power detection technique is explained, it is experimentally verified that, this RCS variation is required to be able to detect the tag appropriately. This estimated model for the calculation of the impedance of the chip for different distances will help to figure out the maximum read range of the double-power measurement technique that is discussed in the following section.

IV. Utilizing the Proposed Impedance Model in Double-Power Detection Technique

As it was discussed in the previous section, the chip impedance behaves nonlinearly as a function of the transmitted power. Here, we will explain more about taking advantage of this chip property for the detection of the sensor tags.

A. Principle of the Double-Power Detection Technique

The double-power measurement technique for the detection of the sensor tags has been briefly introduced in [18]. Since in many applications, the sensor tag is measured in the outdoor environment where the tag response includes background reflections, one of the significant advantages of this technique is elimination of the need for calibration while detection.

Here, after exploring the nonlinear behavior of the chip impedance in more detail, it is easier to understand how the double-power measurement technique really works. As it is shown in Fig. 4(b), transmitting different powers toward the tag cause different chip impedances and subsequently different RCS values of the tag [Fig. 2(c)]. Thus, for two difference transmitted power values that can guarantee a large variation of the chip impedance, there will be different EM (RCS) responses of the tag. The subtraction of the distinct responses contains the pure tag response with no ambient scatterers. The reason is that the normalized response of the background reflections does not vary as a function of the transmitted power, while the RFID chip impedance has a nonlinear behavior as a function of the transmitted power.

As a proof of concept, we applied the double-power measurement technique for the detection of the strain sensor. For this purpose, the detection of an RFID-enabled strain sensor for which a large variation of the magnitude of the response can be observed when subject to a pulling force is performed utilizing the proposed detection technique.

The strain sensor has been fabricated with the embroidery technology [16] on a stretchable fabric, as it is reported in detail in [11]. The prototype sample of the strain sensor tag, which is used for the double-power measurement technique is shown in Fig. 6(a). The performance of the sewn sensor was experimentally characterized using the bistatic radar technique.

Fig. 6(b) shows the bistatic measurement setup for the detection of the sensor. The strain sensor is vertically placed on the mechanical stretching test bench, at a distance of 30 cm in front of the transmitter and receiver antennas. The transmitter antenna connected to port 1 of the VNA is the vertical polarized Huber–Suhner planar antenna with a gain of 8 dBi (including the cable) in the frequency range of 870–960 MHz. The receiver antenna is also a vertical polarized Huber–Suhner. Its gain is about 7 dBi (including the cable) for the same

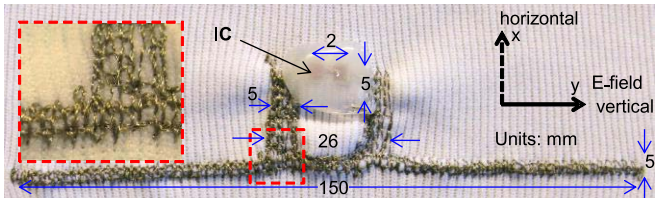

(a)

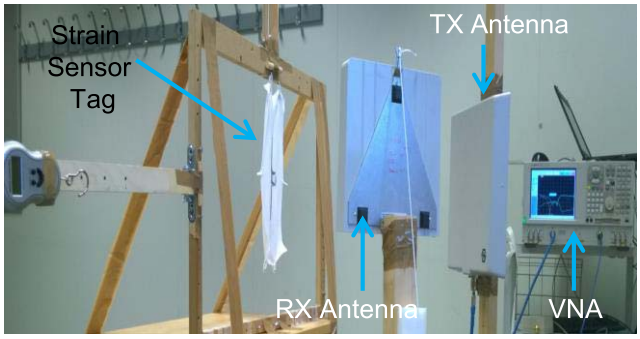

(b)

Fig. 6. (a) Embroidered strain sensor tag. (b) Bistatic radar measurement setup.

frequency range, and it is connected to port 2 of the VNA. The orientation of the transmitter and reader antennas has been achieved to optimize the best performance of the tag.

The scattering parameter S_{21}, contains the EM response of the tag, is measured by applying the tensile force in vertical direction and stretching the fabric, subsequently modifying the length of antenna. The S_{21} of the sensor tag for different antenna's lengths has been measured once for the transmitted power of -5 dBm and then for 14 dBm and it is illustrated in Fig. 7(a). The backscattered signal of the sensor tag for each power level always includes the static reflections from ambient scatterers, since measurement is done in outdoor environment (outside of the anechoic chamber). Basically, these reflections can be removed by the subtraction of the two scattered signals for the two power levels, thus extracting the pure tag response. In this case, no additional background/calibration measurements are needed.

Fig. 7(b) shows the subtraction of the scattering parameters (S_{21}) of two different power levels for each antenna length. As one can see, by increasing the length of the antenna the magnitude of the differential S_{21} is rising and this verifies that the applied strain can be effectively sensed.

Fig. 7(c) shows the sensitivity in terms of the magnitude shift versus percentage of the applied strain at the frequency of 915 MHz. The slop of the best-fit curve gives a sensitivity of 0.36% magnitude shift per 1% strain. However, the purpose of this paper is not the design of a high sensitivity strain sensor, but to show the reliability of the proposed technique for sensing application. Moreover, the higher sensitivity value is achievable at the frequency with higher magnitude variation.

Since we were able to detect the strain with a reasonable sensitivity, at a distance of 30 cm, we have to consider the accuracy of the proposed technique. As shown in Fig. 5, for the measurement distance of 30 cm, and for the selected power

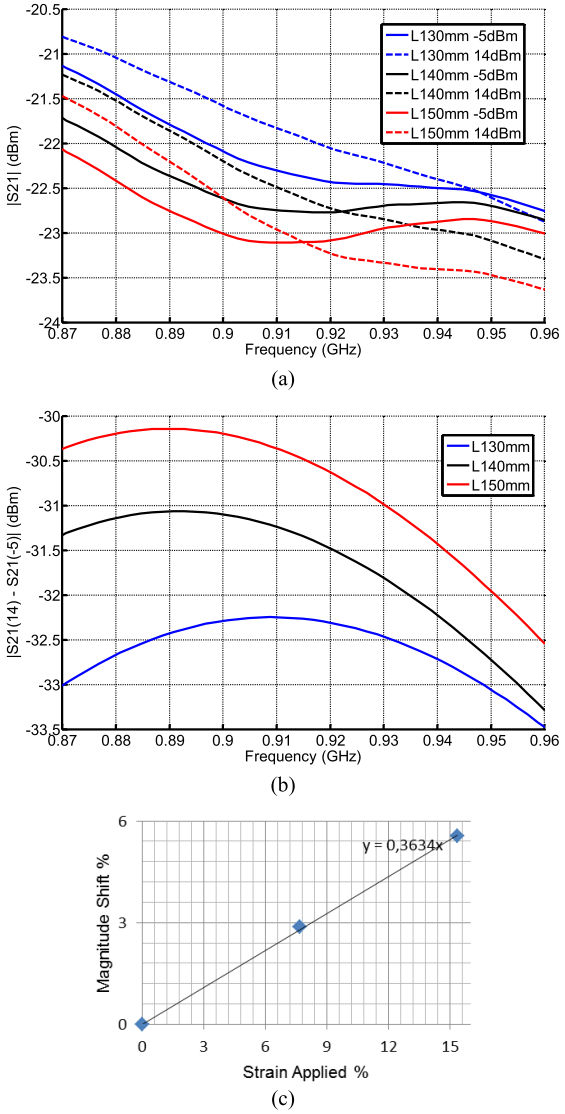

Fig. 7. (a) S_{21} of the strain sensor is measured at a distance of 30 cm, for two different power levels (−5 and 14 dBm) for different strains. (b) Detection of the strain sensor at a distance of 30 cm. (c) Plot of % magnitude shift versus % applied strain in a single frequency of 915 MHz.

levels incident to the tag, the chip impedance significantly varies (163–120 Ω), which can guarantee a very different RCS response. Varying the RCS, between a minimum and maximum value, is the main principle of the detection in the double-power measurement technique. If we assume that the ΔRCS of about 5 is required for a reliable detection, from Fig. 5, we are able to estimate how much are the required minimum and maximum transmitted powers for higher measurement distances.

B. Accuracy of the Proposed Technique

One of the most significant issues, concerning the use of the double-power detection method for practical application measurement, is the maximum read range and the accuracy of this detection method. With respect to the maximum available power ($P_{tx} = 14$ dBm) of the measurement setup, we are able to calculate the maximum read range of the proposed technique using the radar range equation as follows [13]:

$$\frac{P_{rx}^{\min}}{P_{tx}} = \sigma_{\min} \frac{\lambda^2 G_t G_r}{(4\pi)^3 (r_1 r_2)^2} \tag{7}$$

where $\lambda = 0.327$ m is the wavelength and $G_t = 8$ dBi and $G_r = 7$ dBi are the transmitter and receiver antenna's gains, respectively, and σ is the minimum RCS value (−19 dBsm) to have the maximum ΔRCS for an optimal detection.

The power sensitivity level $P_{rx}^{\min}$ represents the threshold power detectable by this radar system and the noise floor often defines its value. The noise floor value for the measurement setup plotted in Fig. 6(b) has been achieved as follows:

$$P_{rx}^{\min} = \text{Max}\{\text{Error}_{n-1}, \ldots, \text{Error}_1\} \tag{8}$$

where the error values are defined according to the following:

$$\begin{aligned} \text{Error}_1 &= S_{21_{\text{BG2}}} - S_{21_{\text{BG1}}} \\ &\vdots \\ \text{Error}_{n-1} &= S_{21_{\text{BG}n}} - S_{21_{\text{BG1}}} \end{aligned} \tag{9}$$

where the $S_{21_{\text{BG}}}$ is the background (no-tag) measurement of the setup in different times. Here, the S_{21} of the background has been measured 100 times ($n = 100$) and after plotting all error curves for the whole frequency band, the maximum curve is selected as the noise floor value. Finally, we obtained a sensitivity value of about −27 dBm.

Substituting all the parameters in (7), and assuming the r_1 (distance between the tag and transmitter antenna) is equal to r_2 (distance between the tag and receiver antenna), the maximum read range of the proposed setup is estimated to be $r^{\max} = 70$ cm.

Based on the results in Fig. 5, we can also see that by keeping the maximum power at 14 dBm and doubling the measurement distance (close to 70 cm), the variation of the impedance is not as large as it was for 30 cm thus, there is no large variation in RCS values as well. Based on the model proposed in Fig. 2(c), a ΔRCS of about 5 dB can guarantee a good detection, while it is not achievable for a small impedance variation. Expanding the technique for higher read range required utilizing other measurement equipment, which can provide higher power value. The section implements the setup with the commercial measurement equipment.

V. Implementation of Model Using Tagformance RFID Measurement System

To study the accuracy of the proposed technique for higher read range, we have used the Tagformance reader and repeated the measurements.

The Tagformance RFID measurement system is a bistatic reader unit containing an RF generator and an RF receiver. The reader offers a transmitted output power of 3–27 dBm over the frequency range of 800 MHz–1 GHz. For the typical tag measurements, the Tagformance software does a threshold sweep, which calculates the minimum power level that is required to activate a tag. Practically, the software does a frequency sweep from 800 to 1000 MHz with adjustable steps (i.e., 5 MHz). At each frequency, the transmit power is varying

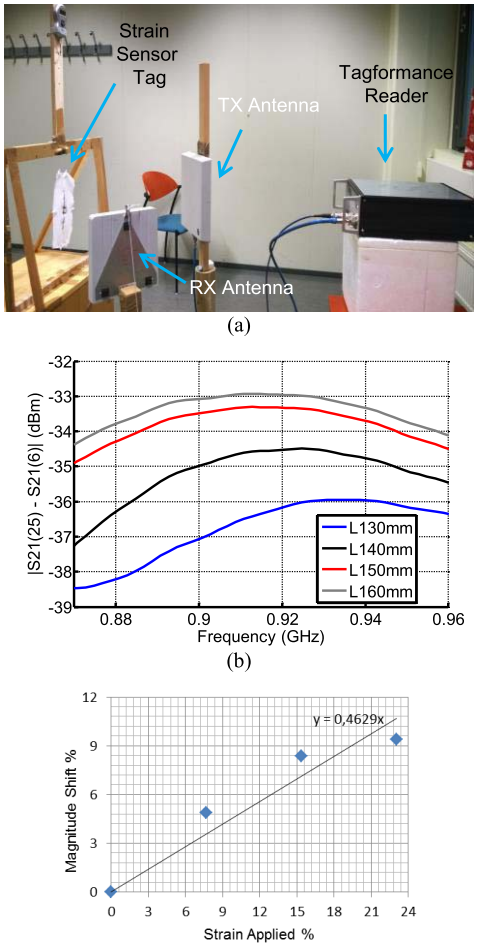

Fig. 8. (a) Replacing the VNA with Tagformance reader in bistatic radar measurement setup. (b) Detection of the strain sensor at 150 cm. (c) Plot of % magnitude shift versus % applied strain in a single frequency of 915 MHz.

in 0.1-dB steps (or in 0.5 and 1-dB steps) to find the lowest power for which the tag is responding. Thus, the transmitted power required to activate the tag varies with the frequency.

Since we are not using any specific protocol in our measurement setup, we did not use this feature of Tagformance software. In fact, here, the Tagformance reader is only used as a transceiver hardware that can provide power levels up to 27 dBm. We have programmed the Tagformance using the LabView, in the way that we can adjust the transmitted power for having the maximum read range and measure the response of the sensor tag. The S_{21} is calculated using LabView code as well.

Fig. 8(a) shows the new measurement setup using Tagformance instead of VNA. The strain sensor has been placed in front of the reader antenna at a distance of 150 cm. From Fig. 5, the minimum and maximum power levels of 6 and 25 dBm, which can guarantee the sufficient ΔRCS for the detection have been adjusted. The S_{21} of the sensor tag for different antenna lengths has been measured for both power levels, and differential-S_{21} for each applied strain are plotted in Fig. 8(b). The magnitude shift shows the detection of the strain as it was expected. The calculated sensitivity percentage is also plotted in Fig. 8(c) and its value is comparable with the measurement at 30 cm.

The maximum Effective Isotropic Radiated Power for an operating frequency within the UHF band around 915 MHz, defined by the federal communication commission (FCC), is 36 dBm. Using (7), the maximum detection range of the radar measurement setup is about 2.5 m, which was estimated based on the estimated results in Fig. 5.

VI. Conclusion

In this paper, we have presented a novel way to estimate the nonlinear variation of RFID chips' impedance values as a function of the transmitted power levels as well as a novel embroidered flexible RFID-enabled wireless platform for repeatable strain sensing measurement in a variety of rugged environment. The method, which relies on the double-power detection, is able to detect the sensed parameter of the sensor based on the nonlinear properties of the RFID chip as a function of the incident power. This method relies upon the detection of the backscattered response for two distinct transmitting power levels and then calculating the difference of these two responses. The nonlinearity of the chip causes a large variation of its impedance value and thus a large difference of RCS values enabling a reliable operability over different measurement ranges.

Acknowledgment

The authors would like to thank J. Tuominen, CTO at Voyantic Oy., for the help with Tagformance reader programming.

References

[1] K. Finkenzeller, *RFID Handbook: Fundamentals and Applications in Contactless Smart Cards, Radio Frequency Identification and Near-Field Communication*. New York, NY, USA: Wiley, 2010.

[2] A. Rida, L. Yang, and M. M. Tentzeris, *RFID-Enabled Sensor Design and Applications* (Integrated Microsystems). Norwood, MA, USA: Artech House, 2010.

[3] R. Bhattacharyya, C. Floerkemeier, S. Sarma, and D. Deavours, "RFID tag antenna based temperature sensing in the frequency domain," in *Proc. IEEE Int. Conf. RFID*, Apr. 2011, pp. 70–77.

[4] S. Andreev, O. Galinina, and Y. Koucheryavy, "Energy-efficient client relay scheme for machine-to-machine communication," in *Proc. IEEE Globecom*, Dec. 2011, pp. 1–5.

[5] S. Andreev, Y. Koucheryavy, N. Himayat, P. Gonchukov, and A. Turlikov, "Active-mode power optimization in OFDMA-based wireless networks," in *Proc. IEEE Globecom Workshop*, Dec. 2010, pp. 799–803.

[6] S. Manzari, C. Occhiuzzi, S. Nawale, A. Catini, C. Di Natale, and G. Marrocco, "Polymer-doped UHF RFID tag for wireless-sensing of humidity," in *Proc. IEEE Int. Conf. RFID*, Apr. 2012, pp. 124–129.

[7] T. T. Thai, H. Aubert, P. Pons, G. R. DeJean, M. M. Tentzeris, and R. Plana, "Novel design of a highly sensitive RF strain transducer for passive and remote sensing in two dimensions," *IEEE Trans. Microw. Theory Techn.*, vol. 61, no. 3, pp. 1385–1396, Mar. 2013.

[8] S. Caizzone and G. Marrocco, "RFID grids: Part II-experimentations," *IEEE Trans. Antennas Propag.*, vol. 59, no. 8, pp. 2896–2904, Aug. 2011.

[9] S. Manzari, C. Occhiuzzi, S. Nawale, A. Catini, C. Di Natale, and G. Marrocco, "Humidity sensing by polymer-loaded UHF RFID antennas," *IEEE Sensors J.*, vol. 12, no. 9, pp. 2851–2858, Sep. 2012.

[10] R. Bhattacharyya, C. Floerkemeier, and S. Sarma, "RFID tag antenna based sensing: Does your beverage glass need a refill?" in *Proc. IEEE Int. Conf. RFID*, Apr. 2010, pp. 126–133.

[11] M. Hasani, A. Vena, L. Sydanheimo, L. Ukkonen, and M. M. Tentzeris, "Implementation of a dual-interrogation-mode embroidered RFID-enabled strain sensor," *IEEE Antennas Wireless Propag. Lett.*, vo. 12, no. 1536-1225 pp. 1272–1275, Oct. 2013.

[12] W. Wiesbeck and D. Kahny, "Single reference, three target calibration and error correction for monostatic, polarimetric free space measurements," *Proc. IEEE*, vol. 79, no. 10, pp. 1551–1558, Oct. 1991.
[13] C. A. Balanis, *Antenna Theory Analysis and Design*, 2nd ed. New York, NY, USA: Wiley, 2005.
[14] A. Vena *et al.*, "Design and realization of stretchable sewn chipless RFID tags and sensors for wearable applications," in *Proc. IEEE Int. Conf. RFID*, Apr. 2013, pp. 176–183.
[15] B. Zhang, Z. Zhou, K. Zhang, G. Yan, and Z. Xu, "Sensitive skin and the relative sensing system for real-time surface monitoring of crack in civil infrastructure," *J. Intell. Mater. Syst. Struct.*, vol. 17, no. 10, pp. 907–917, 2006.
[16] E. Moradi, T. Bjorninen, L. Ukkonen, and Y. Rahmat-Samii, "Characterization of embroidered dipole-type RFID tag antennas," in *Proc. IEEE Int. Conf. RFID-Technol. Appl. (RFID-TA)*, Nov. 2012, pp. 248–253.
[17] A. Vena *et al.*, "An embroidered two-dimensional chipless strain sensor for wireless structural deformation monitoring," *IEEE Sensors*, vol. 13, no. 12, pp. 4627–4637, Dec. 2013.
[18] M. Hasani, A. Vena, L. Sydanheimo, L. Ukkonen, and M. M. Tentzeris, "A novel RFID-enabled strain sensor using the double power measurement technique," in *Proc. IEEE MTT-S Int. Microw. Symp. (IMS)*, Jun. 2014, pp. 1–4.

Masoumeh Hasani, photograph and biography not available at the time of publication.

Arnaud Vena, photograph and biography not available at the time of publication.

Lauri Sydänheimo, photograph and biography not available at the time of publication.

Manos M. Tentzeris, photograph and biography not available at the time of publication.

Leena Ukkonen, photograph and biography not available at the time of publication.